Direct Measurements of the Charge-Recombination Dynamics of Geminate Ion Pairs Formed upon Electron-Transfer Quenching at High Donor Concentration

Eric Vauthey*

Institut de Chimie-Physique de l'Université de Fribourg, Pérolles, CH-1700 Fribourg, Switzerland

Received: June 30, 2000; In Final Form: October 26, 2000

The rate constants of back-electron-transfer (BET) reaction within geminate ion pairs generated upon static ET quenching of cyano-substituted anthracenes by aromatic amines and methoxy-substituted benzenes (MSB) at high concentration in acetonitrile have been measured directly using ultrafast multiplex transient grating spectroscopy. The free energy of BET, ΔG_{BET}, was varied between −3.0 and −0.6 eV, a range corresponding, in principle, to the inverted, barrierless, and normal regimes. When plotted vs ΔG_{BET}, the measured rate constants, k_{BET}, exhibit a large scattering. Good fits of the semiclassical expression for nonadiabatic ET are obtained if the rate constants are sorted according to the electron donor. The resulting electronic coupling matrix elements V are larger and the solvent reorganization energies smaller than those reported for BET within solvent-separated ion pairs, suggesting that BET takes place between ions in contact. However, in the low exergonicity region, the observed BET rate constants are slower than those reported for contact ion pairs formed by charge-transfer excitation. The dynamics of BET within radical pairs generated upon ET quenching of the *N*-methylacridinium cation has also been investigated, and the role of the electrostatic interaction within geminate ion pairs is discussed.

Introduction

Over the past 2 decades, there have been numerous reports of the observation of the Marcus inverted region for electron-transfer (ET) reactions.[1−21] In most cases, the process was either a charge recombination (CR) or a charge shift (CS). There are only a very few cases where this effect has been observed in the primary photoinduced ET.[22]

When CR within geminate ion pairs (GIPs) is discussed, two types of intermediates have to be distinguished: contact ion pairs (CIPs) and solvent-separated or loose ion pairs (SSIPs).[12,23−25] CIPs are generally formed by excitation in the charge-transfer (CT) band of the ground-state complex. They can also be generated upon diffusional ET quenching, when the free energy of this process is small ($\Delta G_{ET} > \sim -0.4$ eV).[26,27]

On the other hand, SSIPs can be formed upon separation of the CIP or upon diffusional ET quenching, when the free energy of this process is sufficiently exergonic ($\Delta G_{ET} < \sim -0.4$ eV).[26] In this case, contact is not a prerequisite for ET. The quencher concentration must be sufficiently low to ensure that the quenching is really diffusional and not static.

The free-energy dependence of CR in SSIPs can be apparently well discussed within the framework of the semiclassical Marcus theory of nonadiabatic ET. In most cases however, the rate constant of back ET (BET) within SSIPs has been determined indirectly from the measured free-ion yield, Φ_{ion}, and by assuming that the rate constant of separation of the GIP into free ions was the same for a series of acceptor/donor (A/D) pairs of similar size.[5−7,11−13,17,20,28] Direct measurements of the free-energy dependence of BET within SSIPs have been performed by Mataga et al.[8] In the barrierless region however, BET was too fast to be determined with a reasonably low quencher concentration and only lower limit values could be deduced.[8]

The free-energy dependence of BET within CIPs is apparently different from that in SSIPs. Direct measurements performed by several groups have shown that the decrease of the BET rate constant with increasing exergonicity is substantially weaker than that predicted by the Marcus theory for the inverted region.[24,27,29−31] Moreover, the normal region is absent; that is, the BET rate constant increases monotonically with decreasing free energy. Several hypotheses have been proposed to explain this discrepancy.[30−32]

We present here a study of the free-energy dependence of the rate constant of BET within GIPs, which are formed by ET quenching of excited acceptors by donor molecules present at high concentration, 1 M, in acetonitrile (ACN). In this case, ET quenching is no longer diffusional, each excited acceptor having a high probability to be in contact with a donor molecule. Consequently, the resulting GIP can be expected to be a CIP rather than a SSIP.

The electron acceptors (A) were cyano-substituted anthracenes (see Chart 1 and Table 1), whereas the donors (D) were either methoxy-substituted benzenes (MSB) or aromatic monoamines (AMA) and diamines (see Chart 2 and Table 2). With these A/D pairs, the free energy of BET, ΔG_{BET}, could be varied from −3.0 to about −0.6 eV. The rate constants of BET, k_{BET}, were determined directly by monitoring the decay of the GIP population using ultrafast multiplex transient grating (TG) spectroscopy. This technique was preferred to the more conventional transient absorption spectroscopy for its superior sensitivity.[33] To have a sufficiently large set of data, the CR dynamics of GIPs with other electron acceptors (see Chart 1) has also been measured.

An investigation of CS within geminate radical pairs (GRP) generated by ET quenching of the *N*-methylacridinium cation (see Chart 1) by various donors is also presented. The role of electrostatic interaction will be studied by comparing the free-energy dependence of CS in GRPs and that of CR in GIPs.

* To whom correspondence should be addressed. E-mail: eric.vauthey@unifr.ch.

10.1021/jp0023260 CCC: $20.00 © 2001 American Chemical Society
Published on Web 12/22/2000

CHART 1: Electron Acceptors

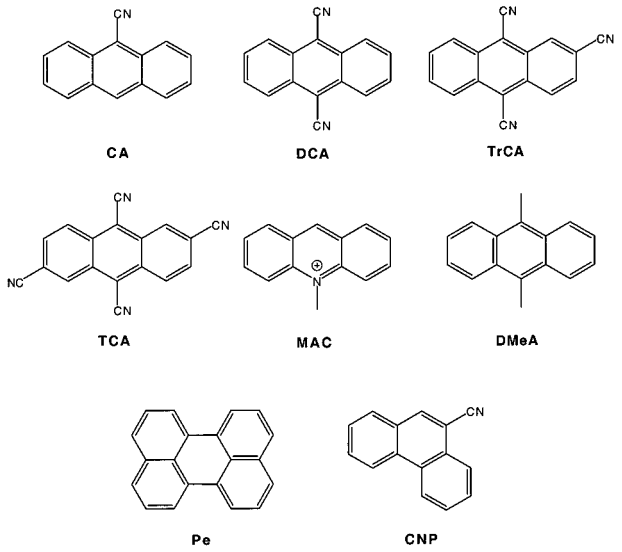

TABLE 1: Excited State Energy, $E(S_1)$, Reduction Potential, E_{red}, and Central Pump Wavelength, λ_{pump}, of the Electron Acceptors

acceptor	$E(S_1)$ (eV)	E_{red} (V vs SCE)	λ_{pump} (nm)
CA	2.96[a]	−1.39[a]	403
DCA	2.88[a]	−0.98[a]	400
TrCA	2.89[b]	−0.70[b]	402
TCA	2.82[c]	−0.45[c]	404
MAC	2.77[c]	−0.46[c]	410
DMeA	3.08[d]	−1.98[e]	400
Pe	2.83[d]	−1.66[e]	408
CNP	3.42[a]	−1.88[a]	355

[a] Reference 34. [b] Reference 11. [c] Reference 35. [d] Reference 36. [e] Reference 37.

CHART 2: Electron Donors

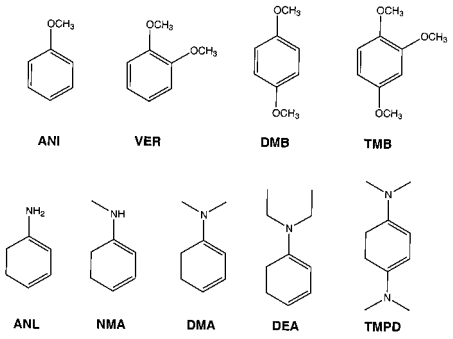

Experimental Section

Apparatus. The multiplex TG setup is shown in Figure 1. The laser pulses were produced at 1 kHz by a Ti:sapphire regenerative amplifier (1; Spectra-Physics, Spitfire LCX), pumped by a Nd:YLF laser (2; Spectra-Physics, Merlin LCX), and seeded by the output of a Ti:sapphire oscillator (3; Spectra-Physics, Tsunami), itself pumped by a Nd:YVO_4 laser (4; Spectra-Physics, Millenia). The pulses produced by this system had 120 fs duration fwhm and an energy of about 250 μJ between 780 and 840 nm. This output was then frequency doubled in a 0.5 mm thick BBO crystal (5). The blue pulses, the pump pulses, were then split into two equal parts, Pu1 and Pu2, which were sent along adjustable optical delay lines (6) before being focused by a 500 mm achromatic lens (7). These pulses were crossed with an angle of 1.2° on the sample (8), located 50 mm in front of the focal point. About 10% of the unconverted

TABLE 2: Oxidation Potential, E_{ox}, Adiabatic Ionization Potential, aIP, and the Difference between the Vertical and Adiabatic Ionization Potentials, ΔIP, of the Electron Donors

donor	E_{ox} (V vs SCE)[a]	aIP (eV)	ΔIP (eV)
ANI	1.76	7.10[b]	0.35[b]
VER	1.45	7.80[b]	0.37[b]
DMB	1.34	7.53[b]	0.43[b]
TMB	1.12	7.33[b]	0.52[b]
ANL	0.98	7.65[c]	0.45[c]
NMA	0.78	7.35[c]	0.33[c]
DMA	0.70	7.10[c]	0.32[c]
DEA	0.69	6.95[c]	0.25[c]
TMPD	0.20	6.20[d]	0.55[d]

[a] Reference 38. [b] Reference 39. [c] Reference 40. [d] Reference 36.

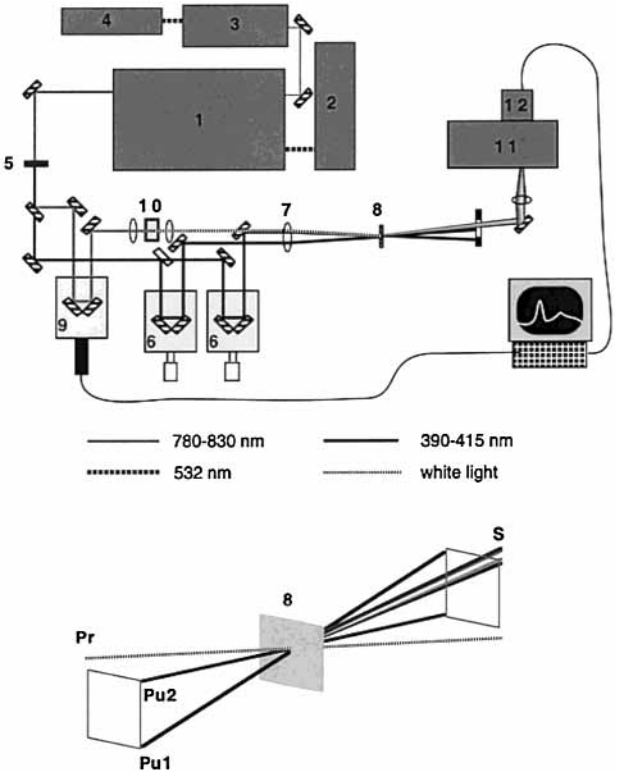

Figure 1. Experimental setup for multiplex TG spectroscopy (top) and beam geometry (bottom; see text for the description of the components).

beam was then sent along an optical delay line, consisting of a computer-controlled motorized translation stage (9; Physik Instrument), before being focused in a 10 mm quartz cell filled with a 70:30 (v/v) D_2O/H_2O mixture for supercontinuum generation (10). The white light pulses, Pr, were recollimated and then focused on the sample to a spot of about 0.5 mm radius by the 500 mm achromatic lens (7). The angle of incidence of the probe pulse on the sample was 0.8°. The two pump pulses and the probe pulse were arranged in a box configuration as shown at the bottom of Figure 1. The polarization of the three incoming beams could be controlled by combinations of a Glan−Taylor polarizer and a half-waveplate. The polarization of the pump pulses was oriented at magic angle relative to that of the probe pulse. The diffracted signal, S, was passed through a cutoff filter (Schott CG 430) to eliminate the scattered pump light and was then focused with a combination of spherical and cylindrical lenses on the entrance slit of a $^1/_4$ m imaging spectrograph (11; Oriel Multispec 257) equipped with a 300 groove/mm grating. As the detector, a 1024 × 256 air-cooled charge-coupled device camera (12; Oriel Instaspec IV) was used. At each position of

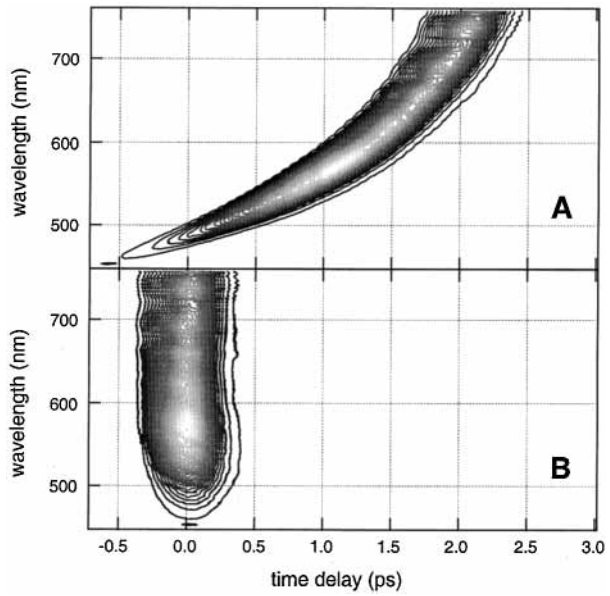

Figure 2. Contour plots of the TG intensity measured upon irradiation of ACN with pulses at 400 nm before (A) and after (B) chirp correction.

the delay line, the TG spectrum was averaged over 1000 shots. For each measurement, the delay line was scanned 10 times. Each measurement was performed three times. The TG spectra were obtained by first subtracting the background spectrum, which was measured by altering the path length of one of the pump pulse to suppress the time coincidence. The ensuing spectra were then corrected through division by the white light pulse spectrum. All TG spectra have been corrected for the chirp of the white light pulses. The latter was determined by monitoring the time dependence of the TG spectrum measured with pure solvent. In this case, the diffracted intensity is due to a phase grating generated by the optical Kerr effect (OKE). Figure 2 shows contour plots of the TG intensity measured with ACN before and after chirp correction.

A detailed description of the TG setup used for excitation at 355 nm can be found in ref 41.

The free-ion yields were determined using photoconductivity.[42] The photocurrent cell has been described in detail elsewhere.[43] The system benzophenone with 0.02 M 1,2-diazabicyclo[2.2.2]octane (DABCO) in ACN, which has a free-ion yield of unity, was used as a standard.[44]

Samples. 9-Cyanoanthracene (CA), 9,10-dicyanoanthracene (DCA; Kodak), 9,10-dimethylanthracene (DMeA), perylene (Pe), and 9-cyanophenanthrene (CNP) were recrystallized. 2,9,10-Tricyanoanthracene (TrCA), 2,6,9,10-tetracyanoanthracene (TCA), and *N*-methylacridinium perchlorate (MAC) were synthesized according to the literature.[45,46] The MSBs anisole (ANI), veratrole (VER), and 1,2,4-trimethoxybenzene (TMB) were distilled, whereas 1,4-dimethoxybenzene (DMB) was recrystallized. The AMAs aniline (ANL), *N*-methylaniline (NMA), *N*,*N*-dimethylaniline (DMA), and *N*,*N*-diethylaniline (DEA) were freshly vacuum distilled on CaH_2, whereas the diamine *N*,*N*,*N*′,*N*′-tetramethyl-1,4-phenylenediamine (TMPD) was sublimed. ACN (UV grade) was used as received. Unless specified, all compounds were from Fluka. The absorbance of the sample solutions at the central excitation wavelength (see Table 1) was around 0.2 over 1 mm, the sample thickness, whereas the donor concentration was 1 M. During the experiment, the sample solutions were continuously stirred by N_2 bubbling. No sample degradation was observed after the measurements. All experiments were performed at 20 ± 1 °C.

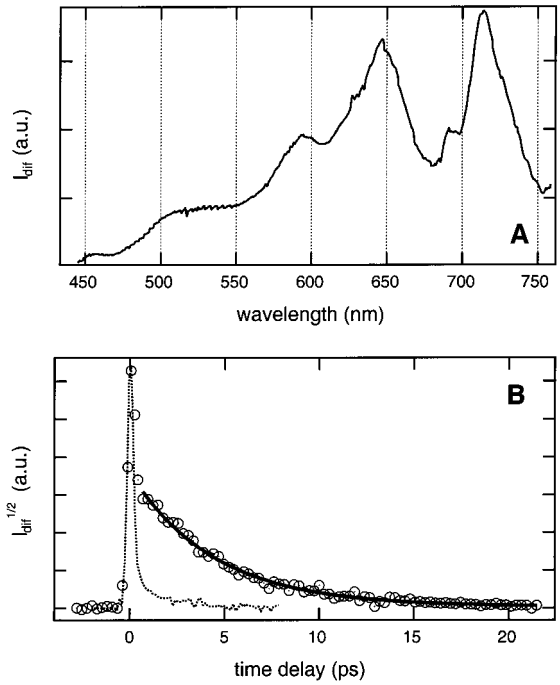

Figure 3. (A) TG spectrum measured with a solution of DCA/DEA in ACN 1 ps after excitation at 400 nm and (B) time profile of the square root of the diffracted intensity at 712 nm measured with the same sample (empty circles), best single-exponential fit (continuous line), and square root of the diffracted intensity due to the nonresonant response of the sample, measured with a 1 M solution of DEA in ACN (dotted line).

Results

Figure 3A shows the chirp-corrected TG spectrum measured with a solution of DCA/DEA in ACN, 1 ps after excitation at 400 nm, whereas Figure 3B shows the time dependence of the square root of the TG intensity at 712 nm. These plots correspond to slices along both the wavelength and time axes in a contour plot similar to that shown in Figure 2B. The nature of a TG spectrum has been examined in detail elsewhere and will only be discussed briefly here.[33,47] According to the Kogelnik coupled wave theory, the relationship between the TG intensity, also called the diffracted intensity, I_{dif}, and the photoinduced optical changes can be described as follows:[48]

$$I_{dif} \propto (\Delta n_r + \Delta n_{nr})^2 + \Delta A^2 \quad (1)$$

where Δn and ΔA are the photoinduced variations of refractive index and absorbance, respectively. In the present case, ΔA is proportional to the concentration of the transient species involved in the photoinduced process. On the other hand, Δn contains two contributions: a resonant one, Δn_r, proportional to the transient population and connected to ΔA through the Kramers−Kronig relationship, and a nonresonant one, Δn_{nr}, which is due to the OKE.[49,50] The OKE arises mainly from the solvent and from D, the concentration of A being too small ([A] ≈ 10^{-4} M) to affect Δn_{nr} significantly. This contribution can be isolated by measuring the diffracted intensity with a 1 M solution of D in ACN. The dotted curve in Figure 3B is the time dependence of the square root of the TG intensity, i.e., of Δn_{nr}, at 712 nm with a 1 M solution of DEA in ACN. The initial spike is due to the electronic OKE, and its time profile corresponds to the third-order correlation of the laser pulses. Thus, at a time delay larger than about 300 fs, its contribution to the signal is zero. The very small remaining intensity arises

from nuclear OKE, and its time dependence reflects the orientational dynamics of the DEA/ACN mixture.

At wavelengths corresponding to absorption maxima, i.e., at 646 and 712 nm for DCA/DEA, Δn_r is essentially equal to zero and $I_{dif} \propto \Delta n_{nr}^2 + \Delta A^2$. The time dependence of ΔA, and hence of the transient population, can be isolated by subtracting the TG intensity measured with D alone in ACN from the TG intensity measured with the solution of A and D. However, Figure 3B shows that after about 300 fs $\Delta A >> \Delta n_{nr}$, and thus this subtraction is only necessary for transients with a decay time shorter than 2 ps. For longer-lived transients, the time dependence of the diffracted intensity is essentially independent of the wavelength, indicating that this subtraction is not required. After a few hundred femtoseconds, the square root of the diffracted intensity reflects the time dependence of the transient population and the TG spectrum is very similar to a transient absorption spectrum.

Coming back to Figure 3A, we see that the TG spectrum corresponds to $DCA^{\bullet-}$, which is formed upon ET quenching of ^{1}DCA* by DEA. The radical cation $DEA^{\bullet+}$ is not observed, because it absorbs only weakly below 500 nm.[51] With the donor concentration used, the ET quenching is so fast that the 620 nm band of ^{1}DCA* cannot be observed. The relative intensities of the TG bands are somewhat different from those reported in ref 27. For the measurements presented here, the crossing angle of the two pump pulses was larger and the spectral bandwidth of the grating was substantially smaller, amounting to about 200 nm. This might somewhat influence the relative intensities of the TG bands. This effect has, however, no incidence at all on the time dependence of the TG intensity. In principle, this problem could be alleviated by dividing the uncorrected TG spectrum by that due to OKE in pure solvent and not by the spectrum of the white light pulses. The time dependence of the square root of the diffracted intensity shown in Figure 3B corresponds to the geminate CR of $DCA^{\bullet-}$ with $DEA^{\bullet+}$. This time profile can be fitted very well with a monoexponential function decaying to zero with a rate constant of k_{GIP}. The deactivation pathways of a GIP are BET and separation into free ions. This last channel is not operative for the DCA/DEA pair, because the TG intensity decays exponentially to zero. If free ions were formed, the TG intensity would decrease to a constant positive value, whose magnitude would reflect the free-ion concentration. For DCA/DEA, a free-ion yield of only 1% has been reported,[7] in agreement with the GIP dynamics measured here. Consequently, for this A/D pair, the rate constant of BET, k_{BET}, is basically identical to k_{GIP} and amounts to 2.5×10^{11} s^{-1}.

TG spectra similar to that shown in Figure 3A have been measured with all of the other donors used, with the exception of TMPD, for which a TG band, centered around 625 nm and ascribed to $TMPD^{\bullet+}$,[51] was observed. In all cases, the square root of the TG intensity decayed monoexponentially to a value very close to zero, which is in agreement with the small free-ion yields reported in ref 7 The measured rate constants, k_{BET}, are listed in Table 3.

TG spectra obtained with the other acceptors—CA, TrCA, TCA, and MAC—are shown in Figure 4. All bands can be ascribed to the reduced acceptor,[29,51,52] and similar spectra have been obtained with all donors, except with TMPD. The TG spectra with DMeA, Pe, and CNP also contain bands from the radical anion and/or from $TMPD^{\bullet+}$. Apart from a few exceptions, the time profile of the TG intensity could be fitted well with a monoexponential function decaying to zero. These exceptions were some GIPs formed by ET quenching of ^{1}CA* and ^{1}CNP*. In these cases, the TG intensity decreased exponentially to a positive value, which remained constant in the time window of the experiment. This residual intensity can be assigned to free ions, because for these A/D pairs Φ_{ion} values larger than 3% have been measured (see Tables 3 and 4). For these pairs, k_{sep}, the rate constant of separation into free ions, and k_{BET} were calculated using the following equation:

$$\Phi_{ion} = \frac{k_{sep}}{k_{GIP}} = \frac{k_{sep}}{k_{sep} + k_{BET}} \qquad (2)$$

TABLE 3: Kinetic Parameters of the GIPs[a]

	A				
D	CA	DCA	TrCA	TCA	MAC
ANI			1.52 4 0.06	4.76	4.34
VER		3.2 4 0.13	13.7	37.7	50
DMB		7.14	24.4	71.4	80
TMB	1.02 6 0.06	22.2	55.5	125	83
ANL	2.79 5 0.15	34.5	54.0	130	75.7
NMA	2.88 5 0.15	40.8	50.0	111	87.0
DMA	1.70 8 0.15	33.3	50.0	86.9	90.9
DEA	1.13 10 0.12	25	47.6	47.6	86.0
TMPD	111	55.5	52.6	54.0	36.4

[a] The values at the intersection of an A row with a D column correspond to k_{BET} (in 10^{10} s^{-1}), Φ_{ion} (%), and k_{sep} (in 10^{10} s^{-1}) in the first, second, and third positions, respectively, measured with this A/D pair. For pairs with a single value, Φ_{ion} was smaller or equal to 3%; thus, the listed value corresponds to k_{BET} (error on $k_{BET} = \pm 5\%$).

Discussion

Nature of the GIP. CT absorption bands were only observed with pairs containing strong A and D. The maxima of the CT bands are listed in Table 5. This table shows that excitation around 400 nm leads predominantly to the formation of the locally excited acceptor, ^{1}A*. Apart from a few exceptions, this state was not observed. This is certainly due to a very fast ET quenching, favored by the high donor concentration used. ET quenching taking place in less than 100 fs has been observed with acceptor molecules dissolved in electron-donating solvents.[53−55] In the present study, the TG bands of ^{1}A* are probably hidden by the nonresonant response of the solvent.

The free energy of ET quenching was calculated with the following equation:[56]

$$\Delta G_{ET} = E_{ox}(D) - E_{red}(A) - E(S_1) \qquad (3)$$

where E_{ox}(D) and E_{red}(A) are the oxidation and reduction potentials of D and A, respectively, and $E(S_1)$ is the energy of the excited precursor. At this stage of the discussion, the correction term C is neglected.

From the above equation and with the data listed in Tables 1 and 2, it appears that ΔG_{ET} is always more negative than −0.5 eV. Therefore, the reactions studied here should, in principle, involve only SSIPs.[26] However, with a donor con-

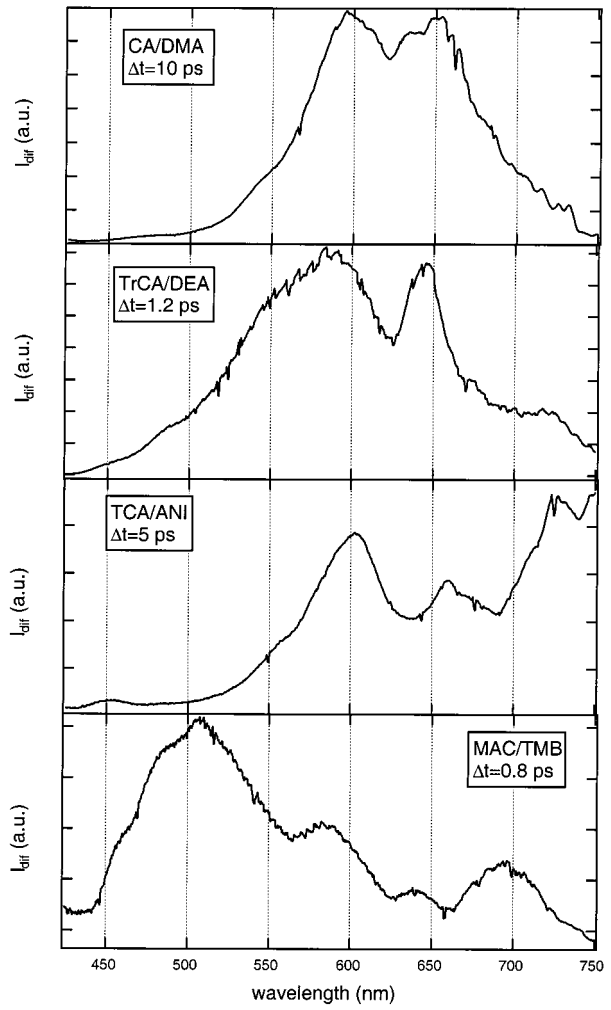

Figure 4. TG spectra measured with different A/D pairs in ACN at various time delays after excitation.

TABLE 4: Kinetic Parameters of GIPs Containing Pe, DMeA, and CNP

A/D	k_{BET} (ns^{-1})	Φ_{ion} (%)	k_{sep} (ns^{-1})
CNP/TMB	0.67	26	0.24
CNP/DMA	0.42	46	0.35
CNP/DEA	0.30	50	0.30
DMeA/TMPD	112	≈0	
Pe/TMPD	400	≈0	

TABLE 5: Maxima of the CT Band, λ_{CT}, Observed with Various A/D Pairs

A/D	λ_{CT} (nm)	A/D	λ_{CT} (nm)	A/D	λ_{CT} (nm)
CA/TMPD	450	TrCA/TMPD	650	TCA/DMA	572
DCA/DMA	470	TCA/TMB	500	TCA/DEA	602
DCA/TMPD	560	TCA/ANL	500	TCA/TMPD	764
TrCA/DMA	509	TCA/NMA	546		

centration of 1 M, the quenching is no longer diffusional, and the ensuing ions must not be solvent-separated but rather in contact. The use of eq 2 to extract k_{sep} and k_{BET} from k_{GIP} for A/D pairs with a substantial free-ion yield (Φ_{ion} > 3%) is only correct if CR within the SSIP is negligible. According to direct investigations of CIP dynamics, the involvement of SSIPs in CR is characterized by a biexponential decay of the IP population, with the faster decay corresponding to the CIP and the slower one to the SSIP.[57−59] Because the decay of the GIP population measured here was monoexponential, the assumption

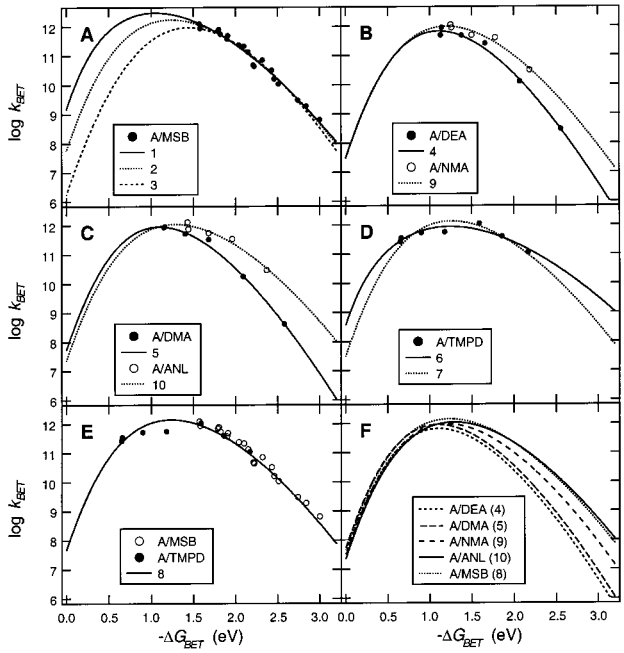

Figure 5. (A)−(E) Rate constants of BET sorted according to the donor and best fits of eq 4. (F) Comparison of the calculated curves. The numbers in the legends refer to the parameters listed in Table 7.

of negligible CR in SSIP seems reasonable. In principle, a monoexponential decay of the GIP population could also be interpreted as a fast conversion of CIP into SSIPs followed by CR in the SSIP. However, from an investigation of the deuterium effect on the dynamics of CIPs composed of DCA and weak donors, it could be shown that the free-ion yield was essentially determined by the competition, within the CIP, between CR and separation into free ions and that the role of SSIPs was negligible.[60]

On the other hand, GIPs with a smaller free-ion yield (Φ_{ion} < 3%) decay predominantly by ultrafast CR, and thus $k_{GIP} \approx k_{BET}$. Because CR is much faster than diffusion, the BET distance must be essentially the same as the ET quenching distance. Consequently, the CR processes investigated here must take place at a contact distance.

***k*BET Values Sorted According to A.** A plot of the k_{BET} values listed in Tables 3 and 4 as a function of the free energy of BET, calculated as $\Delta G_{BET} = E_{red}(A) - E_{ox}(D)$, shows a large scattering of the data. Apparently much better correlations are obtained if the k_{BET} values are sorted according to the electron acceptor, with the exception of the A/TMPD pairs. These correlations can be fitted with parabolas, as predicted by the purely classical Marcus theory.[61] However, the theoretical parameters obtained from a fit of the classical Marcus expression change substantially from one acceptor to another in a way that is very difficult to account for. Moreover, reasonable fits are only possible if the k_{BET} values measured with the A/TMPD pairs are omitted, and there is no reasonable explanation to justify this.

***k*BET Values Sorted According to D.** Figure 5 shows the measured k_{BET} values sorted according to the electron donor. The continuous lines are the best fits of the following semiclassical expression for nonadiabatic ET:[61,62]

$$k_{BET} = \frac{2\pi}{\hbar} V^2 (4\pi\lambda_s k_B T)^{-1/2} \sum_{n=0}^{\infty} \frac{S^n}{n!} \exp(-S) \exp\left[\frac{\Delta G_{BET} + nh\nu + \lambda_s}{4\lambda_s k_B T}\right] \quad (4)$$

TABLE 6: Parameters Obtained from the Fit of Equation 4 to the k_{BET} Data Sorted According to the Donor[a]

A/D	V (cm^{-1})	λ_s (cm^{-1})	$\lambda_v(Sh\nu)$ (eV)	
A/MSB	137	0.53	0.60	1
	88	0.90[b]	0.41	2
	73	1.20[b]	0.26	3
A/DEA	58	0.90	0.25	4
A/DMA	68	0.87	0.28	5
A/TMPD	80	0.40	0.93	6
	89	0.90[b]	0.42	7
A/MSB−TMPD	92	0.86	0.44	8
A/NMA	73	0.90[b]	0.36	9
A/ANL	81	0.90[b]	0.45	10

[a] The vibrational frequency was fixed at 1500 cm^{-1}. The numbers in the last column correspond to the calculated curves shown in Figure 5. [b] λ_s was fixed at this value during the fit.

where V is a matrix element describing the electronic coupling between the initial and final states, λ_s is the reorganization energy associated with solvent modes and other low-frequency intramolecular modes, ν is the average frequency of the modes coupled to ET, and S is the Huang−Rhys factor, which can be considered as the average number of vibrational quanta excited in the final state:

$$S = \frac{\lambda_v}{h\nu} \tag{5}$$

with λ_v being the reorganization energy associated with high-frequency intramolecular modes.

For the fit, $h\nu$ was fixed at 0.186 eV, which corresponds to a vibrational frequency of 1500 cm^{-1}.

The rate constants for pairs containing MSB donors correlate very well with ΔG_{BET} and decrease markedly with increasing exergonicity (see Figure 5A). The resulting parameters of the fit of eq 4 are listed in Table 6. Despite a rather large free-energy range, the curvature of the free-energy dependence is not pronounced enough to allow a univocal set of parameters to be extracted. Table 6 shows other sets of parameters obtained by fixing the value of λ_s during the fitting procedure (see also Figure 5A). A value of λ_s higher than 1.2 eV results in a curve that clearly does not fit the experimental data.

Although the MSBs seem to behave similarly, the situation is substantially different with the AMAs and TMPD. Figure 5 shows that the BET rate constants in GIPs containing ANL, NMA, DMA, DEA, and TMPD exhibit clearly a different free-energy dependence. To have enough data to perform a fit of eq 4, the k_{BET} values measured in GIPs with Pe, CNP, and DMeA as electron acceptors are also reported. Although the AMAs are structurally similar, k_{BET} decreases continuously with increasing substitution on the nitrogen atom, independently of the acceptor, i.e., independently of the free-energy domain where CR takes place. The parameters obtained from the best fit of eq 4 to the BET rate constants measured in the A/DMA, A/DEA, and A/TMPD pairs are listed in Table 6, and the corresponding fits are shown in Figure 5. For the A/TMPD pairs, the curvature of the free-energy dependence is too weak to allow a reliable determination of the theoretical parameters. However, the rate constants measured with the A/TMPD pairs present apparently the same ΔG_{BET} dependence as those found with the A/MSB pairs (see Figure 5E). Grouping the data measured with these two sets of GIPs allows a better fit of eq 4. The resulting parameters are now more consistent with those obtained with the A/DMA and A/DEA pairs. From these fits, it appears that the solvent reorganization energy is almost constant. Because the number of experimental points for the A/NMA and A/ANL pairs is small, the λ_s value was fixed to 0.90 eV during the fitting procedure, and only V and S were allowed to vary.

According to the best-fit parameters listed in Table 6, both V and λ_v vary substantially with the nature of the donor. For the AMAs, the decrease of V by an increasing substitution on the nitrogen atom is accompanied by a parallel increase of λ_v. It is reasonable to assume that the contribution of the acceptor to λ_v must be about the same for all cyanoanthracenes. In principle, the magnitude of this energy can be estimated from the band shape of the electron transmission spectrum of A.[63] Such spectra are not known, but those of benzene and naphthalene have been reported.[64] For these two molecules, λ_v is on the order of 0.2 eV.[64] It is therefore reasonable to assume a similar reorganization energy for the acceptors used here. Similarly, the intramolecular reorganization energy associated with the neutralization of $D^{\bullet+}$ can be deduced from the band shape of the photoelectron spectrum of D, i.e., from the difference between its vertical and adiabatic ionization potentials, ΔIP.[65] As shown in Table 2, ΔIP decreases almost continuously by going from ANL to DEA, which is in agreement with the λ_v values obtained from the fit. Amines are known to have a pyramidal structure around the N atom. However, this structure is planar in the ionized state, and the reorganization energy corresponds mainly to this structural change. The extent of pyramidalization of the N atom in the neutral amine depends on the size of the substituents. Neutral amines with three bulky substituents, like triisopropylamine or triphenylamine, are known to have a planar structure around the N atom.[66,67] Thus, for such amines, the reorganization energy upon ionization is small. Consequently, the decrease of ΔIP, and hence of λ_v, observed by going from ANL to DEA might be ascribed to a decrease of the pyramidalization angle in the neutral amine by going from H to ethyl substituents.

The decrease of V with an increasing substitution on the N atom is probably due to the effect of charge dilution. In the radical cation, the positive charge becomes more delocalized as the size of the substituents increases, and the wave functions involved in the CR are more diffuse in $DEA^{\bullet+}$ than in $ANL^{\bullet+}$. Consequently, the electronic-coupling matrix element V, which depends on the overlap of the wave functions of $A^{\bullet-}$ and $D^{\bullet+}$, becomes smaller. Such an effect has been invoked in a recent investigation on the influence of steric crowding on the CR dynamics within GIPs containing aliphatic amines.[68] The observed decrease of k_{BET} with the increasing size of the substituents on the N atom was too large to be entirely explained by the effect of steric hindrance.

If the substitution of the AMAs has such a strong influence on k_{BET}, one wonders why this is not also the case with the MSBs. The ΔIP values listed in Table 2 indicate that λ_v increases with the number of methoxy substituents. It is reasonable that, if each methoxy group undergoes some structural change upon ionization, the total reorganization energy increases with the number of groups.

The electronic-coupling matrix element V can be expected to decrease with the number of methoxy substituents for the reason discussed above with the AMAs. With the amines, this decrease of V was accompanied by a parallel *decrease* of λ_v. With the MSBs, this decrease of V is predicted to occur with an *increase* of λ_v.

As was already mentioned above, the k_{BET} values measured with MSBs lie in the inverted region, and the fit of eq 4 does not result in very reliable values of V and λ_v. At constant λ_s, reasonably good fits can be obtained with different sets of V

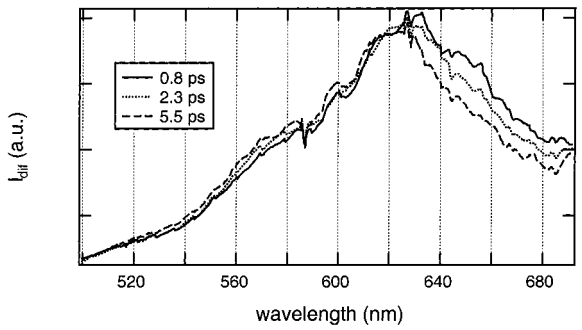

Figure 6. Intensity-normalized TG spectra measured with TCA/TMPD at various time delays after excitation.

and λ_v, with a decrease of λ_v being compensated by an increase of V. Therefore, we think that the single free-energy dependence observed with the A/MSB pairs is fortuitous. For the reasons discussed above, the λ_v value for the A/ANI pairs must be smaller than that for the A/TMB pairs. However, the resulting decrease of k_{BET} in the A/ANI pairs is completely counterbalanced by a larger V. This compensation effect does not occur with the AMAs because both V and λ_v decrease with increasing substitution.

Table 2 shows that the reorganization energy related to the neutralization of $TMPD^{\bullet+}$ is very large. This energy is associated with important structural changes upon ionization. Indeed resonance Raman studies have revealed that $TMPD^{\bullet+}$ has a quinoidal structure.[69] This indicates that there is a strong conjugation of the *n*-electron pairs of the N atoms to the π electron of the ring. This effect might be at the origin of the relatively large V. Nevertheless, Figure 5D shows that the fit of eq 4 to the k_{BET} values measured with the A/TMPD pairs is much poorer that those obtained with other pairs. A possible reason for this relatively bad fit is that the corresponding GIPs, especially those with TrCA, TCA, and MAC, are generated in highly exergonic ET quenching reactions. For TCA/TMPD, ΔG_{ET} amounts to -2.11 eV and CR takes place with a time constant of 1.8 ps. Kaiser and co-workers have shown that the vibrational cooling time of a molecule in solution increases with increasing excess excitation energy.[70] For example, the vibrational cooling time measured with a dye molecule in ethanol, excited with 2.1 eV of excess energy, is 6 ps.[70] It is thus highly probable that CR takes place while the ions are still vibrationally hot. In principle, hot molecules are characterized by a broadening of the red side of the absorption band. The TG spectra with A/TMPD pairs exhibit mainly the broad 625 nm band of $TPMD^{\bullet+}$. Figure 6 shows intensity-normalized TG spectra measured with the TCA/TMPD pair at different time delays after excitation. The TG intensity decreases apparently more rapidly on the red side of this band. Indeed, the decay time on the red side is 7.5% shorter than that at the band maximum. The temperature of a GIP with an excess energy of 2.1 eV can be estimated to be around 600 K. The effect of temperature on k_{BET} depends strongly on ΔG_{BET}. In the inverted regime, the temperature dependence of k_{BET} is small, with BET being essentially a nonradiative transition. In the barrierless region, k_{BET} should, in principle, exhibit a slight decrease with increasing temperature.[71] Finally in the normal region, the BET is an activated process, with the barrier height increasing with diminishing exergonicity. Consequently, the formation of hot GIPs should only have a marked influence on the k_{BET} values situated in the normal region, i.e., for BETs which are less exergonic than about -1 eV. In these few cases, the k_{BET} values measured here might be larger than those for thermally equilibrated GIPs.

Electrostatic Interaction. In principle, eq 3 should contain an additional correction factor C, often called the Coulomb term, taking into account the energy gained by bringing the two radical ions at ET distance.[56] This term contains a contribution from the electrostatic interaction and one from the solvation energy, the relative magnitude of which is still a subject of controversy.[72,73] In the case of MAC, the ET quenching is a CS, and there is no electrostatic stabilization of the ensuing GRP. Therefore, if this interaction is strong in a GIP, ΔG_{BET} for MAC/D pairs should differ from ΔG_{BET} for TCA/D pairs, although these two acceptors have the same reduction potential. Table 3 shows that the k_{BET} values measured with MAC/D and TCA/D pairs do not differ substantially. The free-energy dependencies of k_{BET} are comparable, with the fastest BET occurring at $\Delta G_{BET} \approx -1.40$ eV. There are two possible explanations for this similarity: (1) The electrostatic interaction is small, and thus $\Delta G_{BET}(MAC/D) \approx \Delta G_{BET}(TCA/D) \pm 0.1$ eV. (2) The electrostatic interaction is substantial, and $\Delta G_{BET}(MAC/D) < \Delta G_{BET}(TCA/D)$. However, the effect of this difference on k_{BET} is compensated by a change of λ_s, with $\Delta G_{BET} + \lambda_s$ remaining constant. The electrostatic stabilization in a GIP composed of a benzophenone anion and $DABCO^{\bullet+}$ has been determined to amount to -0.18 ± 0.08 eV in ACN.[74] A difference in λ_s cannot be ruled out, although the theoretical expression for λ_s, based on the continuum dielectric model, predicts the same reorganization energy for both CR and CS. However, if one considers the molecular nature of the solvent, the reorganization energy associated with the creation or annihilation of a positive charge might be different from that associated with the creation or annihilation of a negative charge.

Comparison with Other Investigations. The above discussion shows that the free-energy dependence of CR within the GIPs investigated here can be discussed reasonably well in terms of the Marcus theory of nonadiabatic ET, once the rate constants have been sorted according to the structure of the reactants. Thus, the free-energy dependence is apparently similar to that reported for CR within SSIPs. However, the parameters V and λ_v are markedly different: (1) The electronic coupling matrix elements V are substantially larger than the value normally found for SSIPs, between 10 and 20 cm^{-1}.[5,7,19,20,75] Consequently, the rate constants measured here in the barrierless regime are faster by more than 1 order of magnitude than those reported for SSIPs. (2) The solvent reorganization energy, λ_s, found here is substantially smaller than that found for SSIPs, where λ_s is typically on the order of 1.5 eV.[5−7,20,28,75] This difference cannot be ascribed to the high donor concentration used here. Even with a concentration of 1 M, the donor to ACN concentration ratio ranges from 5.8% with ANL to 6.2% with TMPD. From the volume ratios of D and ACN and their static dielectric constant, ϵ_s, and under the assumption that the donor/solvent mixture behaves ideally, the dielectric constant of the solution goes from 34.2 with ANL to 31.2 with TMPD. The polarity function of λ_s is of the form $n^{-2} - \epsilon_S^{-1}$, where n is the refractive index. Therefore, the effect of the relatively high donor concentration on this polarity function and on λ_s is negligibly small.

BET rate constants as large as those observed here have already been reported for CR within CIPs generated by CT excitation of the ground-state complex, indicating similar coupling constants.[24,76] Moreover, according to Gould and coworkers, λ_s associated with CR in CIPs can be expected to be smaller than that for SSIPs.[12] These observations support the

assumption that the GIPs generated upon ET quenching with high donor concentrations are indeed CIPs.

The free-energy dependence of CR in CIPs reported in the literature is weaker than that predicted by the Marcus theory for the inverted region.[24,29−31,77] One explanation to account for this effect is that the variation of ΔG_{BET} obtained by going from one CIP to another is accompanied by a systematic change of V and/or λ.[31] Our results support this hypothesis. The choice of A/D pairs is more limited when forming CIPs by CT excitation than when preparing them by static ET quenching. Such a variation of V and λ is difficult to detect when working with a reduced number of A/D pairs. For example, the free-energy dependence of k_{BET} measured here with TrCA/D pairs is almost flat between −2 and −0.9 eV!

Nevertheless, it should be noted that the CIPs formed by static ET quenching may be somewhat different from those generated by CT excitation. These differences may explain why the k_{BET} values measured here in the low exergonicity region ($\Delta G_{BET} >$ −1 eV) are smaller than those reported by Asahi and Mataga for CIPs formed by CT excitation.[24]

The CIPs formed by CT excitation may have tighter structures than those formed by static ET quenching. In binary crystals, the interplanar distance between the constituents of such a complex is around 3.5 Å.[78] If a similar geometry is assumed in liquids, the resulting interionic distance in the CIPs must be very short. The situation might be different for static ET quenching, where a distribution of the mutual orientations of the ions may be present.

The CIPs composed of strong A and D are formed with more excess energy upon static ET quenching than upon CT excitation. If we consider the model proposed by Frantzusov and Tachiya to explain the absence of a normal region for CR of CIPs,[32] a large excess energy requires a substantial cooling of the CIPs before reaching the bottom of the upper adiabatic surface, where the transition to the ground adiabatic surface, i.e., the CR, is the most efficient.

Finally, it should not be forgotten that the above analysis assumes that CR takes place in one type of GIPs only, namely, within the CIPs formed by static ET quenching. As mentioned above, this assumption is based on the observation of a single-exponential decay of the GIP population. However, CR in both CIPs and SSIPs cannot be completely ruled out. In this case, the single-exponential decay would indicate that CR in both CIPs and SSIPs takes place in similar time scales, and consequently, the extraction of the individual rate constants is no longer possible. However, the rate constant of separation of a CIP to a SSIP, often called k_{solv}, has been reported to vary between 2×10^8 and 1×10^{10} s^{-1}.[79] Because this is significantly smaller than most of the k_{GIP} values measured here (at least 39 of the 46 GIPs), the BET distance must be essentially the same as the ET quenching distance. Even if the analysis is performed with these 39 pairs only, the trends remain qualitatively the same.

Conclusions

From the above discussion, it appears that the GIPs generated upon static ET quenching of A* in the presence of high concentrations of D are closer to CIPs than to SSIPs. The free-energy dependence of CR within these GIPs can be discussed reasonably well in terms of the Marcus nonadiabatic ET theory if the BET rate constants are sorted according to the electron donor. The structural differences between these donors are large enough to lead to different electronic coupling constants and reorganization energies. On the other hand, such differences are apparently not as marked with the electron acceptors, which are all large and rigid aromatic hydrocarbons. Nevertheless, small variations of V and λ by changing the acceptor cannot be excluded.

Although BETs at free energies of up to −0.6 eV have been measured, the normal region was not really observed. In this region, however, the measured rate constants are smaller than those reported for CIPs generated by CT excitation. A detailed investigation on the effect of the excitation wavelength on CR dynamics in this low exergonicity regime is planned.

Acknowledgment. We thank Mr. Jean-Luc Roulin for the synthesis of TrCA, TCA, and MAC as well as for the purification of many compounds. This work was supported by the Fonds National Suisse de la Recherche Scientifique through Project No. 2000-055388.98. Financial support from the Fonds de la Recherche and the Conseil de l'Université de Fribourg is also acknowledged.

References and Notes

(1) Miller, J. R.; Beitz, J. V.; Huddleston, R. K. *J. Am. Chem. Soc.* **1984**, *106*, 5057.
(2) Miller, J. R.; Calcaterra, L. T.; Closs, G. L. *J. Am. Chem. Soc.* **1984**, *106*, 3047.
(3) Wasielewski, M. R.; Niemczyk, N. P.; Svec, W. A.; Pewitt, E. B. *J. Am. Chem. Soc.* **1985**, *107*, 1080.
(4) Irvine, M. P.; Harrison, R. J.; Beddard, G. S.; Leighton, P.; Sanders, J. K. M. *Chem. Phys.* **1986**, *104*, 315.
(5) Gould, I. R.; Ege, D.; Mattes, S. L.; Farid, S. *J. Am. Chem. Soc.* **1987**, *109*, 3794.
(6) Ohno, T.; Yoshimura, A.; Shioyama, H.; Mataga, N. *J. Phys. Chem.* **1987**, *91*, 4365.
(7) Vauthey, E.; Suppan, P.; Haselbach, E. *Helv. Chim. Acta* **1988**, *71*, 93.
(8) Mataga, N.; Asahi, T.; Kanda, Y.; Okada, T.; Kakitani, T. *Chem. Phys.* **1988**, *127*, 249.
(9) Levin, P. P.; Pluzhnikov, P. F.; Kuzmin, V. A. *Chem. Phys. Lett.* **1988**, *147*, 283.
(10) Chen, P.; Duesing, R.; Tapolsky, G.; Meyer, T. J. *J. Am. Chem. Soc.* **1989**, *111*, 8305.
(11) Kikuchi, K.; Takahashi, Y.; Hoshi, M.; Niwa, T.; Katagiri, T.; Miyashi, T. *J. Phys. Chem.* **1991**, *95*, 2378.
(12) Gould, I. R.; Young, R. H.; Moody, R. E.; Farid, S. *J. Phys. Chem.* **1991**, *95*, 2068.
(13) Grampp, G.; Hetz, G. *Ber. Bunsen-Ges. Phys. Chem.* **1992**, *96*, 198.
(14) Kapturkiewicz, A. *Chem. Phys.* **1992**, *166*, 259.
(15) Larson, S. L.; Cooley, L. F.; Elliott, C. M.; Kelley, D. F. *J. Am. Chem. Soc.* **1992**, *114*, 9504.
(16) Yonemoto, E. H.; Riley, R. L.; Kim, Y. I.; Atherton, S. J.; Schmehl, R. H.; Mallouk, T. E. *J. Am. Chem. Soc.* **1992**, *114*, 8081.
(17) Burget, D.; Jacques, P.; Vauthey, E.; Suppan, P.; Haselbach, E. *J. Chem. Soc., Faraday Trans.* **1994**, *90*, 2481.
(18) Weng, Y. X.; Chan, K. C.; Tzeng, B. C.; Che, C. M. *J. Chem. Phys.* **1998**, *109*, 5848.
(19) Jayanthi, S. S.; Ramamurthy, P. *J. Phys. Chem. A* **1997**, *101*, 2016.
(20) Kircher, T.; Löhmannsröben, H.-G. *Phys. Chem. Chem. Phys.* **1999**, *1*, 3987.
(21) Zou, C.; Miers, J. B.; Ballew, R. M.; Dlott, D. D.; Schuster, G. B. *J. Am. Chem. Soc.* **1991**, *113*, 7823.
(22) Prasad, E.; Gopidas, K. R. *J. Am. Chem. Soc.* **2000**, *122*, 3191.
(23) Masnovi, J. M.; Kochi, J. K. *J. Am. Chem. Soc.* **1985**, *107*, 7880.
(24) Asahi, T.; Mataga, N. *J. Phys. Chem.* **1989**, *93*, 6575.
(25) Peters, K. S.; Lee, J. *J. Phys. Chem.* **1992**, *96*, 8941.
(26) Gould, I. R.; Young, R. H.; Mueller, L. J.; Farid, S. *J. Am. Chem. Soc.* **1994**, *116*, 8176.
(27) Vauthey, E.; Högemann, C.; Allonas, X. *J. Phys. Chem. A* **1998**, *102*, 7362.
(28) Jayanthi, S. S.; Ramamurthy, P. *Phys. Chem. Chem. Phys.* **1999**, *1*, 4751.
(29) Asahi, T.; Mataga, N.; Takahashi, Y.; Miyashi, T. *Chem. Phys. Lett.* **1990**, *171*, 309.
(30) Hubig, S. M.; Bockman, T. M.; Kochi, J. K. *J. Am. Chem. Soc.* **1996**, *118*, 3842.
(31) Gould, I. R.; Noukakis, D.; Gomez-Jahn, L.; Goodman, J. L.; Farid, S. *J. Am. Chem. Soc.* **1993**, *115*, 4405.
(32) Frantzusov, P. A.; Tachiya, M. *J. Chem. Phys.* **2000**, *112*, 4216.

(33) Högemann, C.; Pauchard, M.; Vauthey, E. *Rev. Sci. Instrum.* **1996**, *67*, 3449.
(34) *Organic Photochemistry*; Mattes, S. L., Farid, S., Eds.; Dekker: New York, 1983; Vol. 6.
(35) Gould, I. R.; Moser, J. E.; Armitage, B.; Farid, S. *J. Am. Chem. Soc.* **1989**, *111*, 1917.
(36) Murov, S. L.; Carmichael, I.; Hug, G. L. *Handbook of Photochemistry*; Marcel Dekker: New York, 1993.
(37) Parker, V. D. *J. Am. Chem. Soc.* **1976**, *98*, 98.
(38) Siegerman, H. Techniques of Chemistry. In *Techniques of Chemistry*; Weinberg, N. L., Ed.; John Wiley: New York, 1975; Vol. V, p 667.
(39) Jacques, P.; Allonas, X.; Burget, D.; Haselbach, E.; Muller, P.-A.; Sergenton, A.-C.; Galliker, H. *Phys. Chem. Chem. Phys.* **1999**, *1*, 1867.
(40) Maier, J. P.; Turner, D. W. *J. Chem. Soc., Faraday Trans. 2* **1973**, 521.
(41) Vauthey, E. *J. Phys. Chem. A* **1997**, *101*, 1635.
(42) Vauthey, E.; Pilloud, D.; Haselbach, E.; Suppan, P.; Jacques, P. *Chem. Phys. Lett.* **1993**, *215*, 264.
(43) vonRaumer, M.; Suppan, P.; Jacques, P. *J. Photochem. Photobiol., A* **1997**, *105*, 21.
(44) Henseler, A.; Vauthey, E. *J. Photochem. Photobiol., A* **1995**, *91*, 7.
(45) Mattes, S. L.; Farid, S. *J. Am. Chem. Soc.* **1982**, *104*, 1454.
(46) Fukuzumi, F.; Tokuda, Y.; Kitano, T.; Okamoto, T.; Oter, J. *J. Am. Chem. Soc.* **1993**, *115*, 8960.
(47) Högemann, C.; Vauthey, E. *Isr. J. Chem.* **1998**, *38*, 181.
(48) Kogelnik, H. *Bell Syst. Tech. J.* **1969**, *48*, 2909.
(49) Etchepare, J.; Grillon, G.; Chambaret, J. P.; Hamoniaux, G.; Orzag, A. *Opt. Commun.* **1987**, *63*, 329.
(50) Deeg, F. W.; Fayer, M. D. *J. Chem. Phys.* **1989**, *91*, 2269.
(51) Shida, T. *Electronic Absorption Spectra of Radical Ions*; Elsevier: Amsterdam, The Netherlands, 1988; Vol. 34, physical sciences data.
(52) Jones, G., II; Yan, D.-X.; Goztola, D. J.; Greenfield, S. R.; Wasielewski, M. R. *J. Am. Chem. Soc.* **1999**, *121*, 11016.
(53) Wolfseder, B.; Seidner, L.; Domcke, W.; Stock, G.; Seel, M.; Engleitner, S.; Zinth, W. *Chem. Phys.* **1998**, *233*, 323.
(54) Seel, M.; Engleitner, S.; Zinth, W. *Chem. Phys. Lett.* **1997**, *275*, 363.
(55) Xu, Q.-H.; Scholes, G. D.; Yang, M.; Fleming, G. R. *J. Phys. Chem. A* **1999**, *103*, 10348.
(56) Rehm, D.; Weller, A. *Isr. J. Chem.* **1970**, *8*, 259.
(57) Asahi, T.; Mataga, N. *J. Phys. Chem.* **1991**, *95*, 1956.
(58) Ojima, S.; Myasaka, H.; Mataga, N. *J. Phys. Chem.* **1990**, *94*, 7534.
(59) Peters, K. S.; Lee, J. *J. Am. Chem. Soc.* **1993**, *115*, 3643.
(60) Muller, P.-A.; Högemann, C.; Allonas, X.; Jacques, P.; Vauthey, E. *Chem. Phys. Lett.* **2000**, *236*, 321.
(61) Marcus, R. A.; Sutin, N. *Biochim. Biophys. Acta* **1985**, *811*, 265.
(62) Kestner, N. R.; Logan, J.; Jortner, J. *J. Phys. Chem.* **1974**, *78*, 2148.
(63) Allan, M. *J. Chem. Educ.* **1987**, *64*, 418.
(64) Allan, M. *J. Electron Spectrosc. Relat. Phenom.* **1989**, *48*, 219.
(65) Nelsen, S. In *Advances in Electron-Transfer Chemistry 3*; Mariano, P. S., Ed.; JAI Press Inc.: Greenwich, U.K., 1993; Vol. 3, p 167.
(66) Bock, H.; Göbel, I.; Havlas, Z.; Liedle, S.; Oberhammer, H. *Angew. Chem.* **1991**, *103*, 193.
(67) Sakanoue, K.; Motoda, M.; Sugimoto, M.; Sakaki, S. *J. Phys. Chem. A* **1999**, *103*, 5551.
(68) Vauthey, E. *J. Phys. Chem. A* **2000**, *104*, 1804.
(69) Poizat, O.; Bourkba, A.; Buntinx, G.; Deffontaine, A.; Bridoux, M. *J. Chem. Phys.* **1987**, *87*, 6379.
(70) Laermer, F.; Elsaesser, T.; Kaiser, W. *Chem. Phys. Lett.* **1989**, *156*, 381.
(71) Bagchi, B.; Oxtoby, D. W.; Fleming, G. R. *Chem. Phys.* **1984**, *86*, 257.
(72) Suppan, P. *J. Chem. Soc., Faraday Trans. 1* **1986**, *82*, 509.
(73) Tachiya, M. *Chem. Phys. Lett.* **1994**, *230*, 491.
(74) Vauthey, E.; Henseler, A. *J. Photochem. Photobiol., A* **1998**, *112*, 103.
(75) Kikuchi, K.; Takahashi, Y.; Koike, K.; Wakamatsu, K.; Ikeda, H.; Miyashi, T. *Z. Phys. Chem. Neue Folge* **1990**, *167*, 27.
(76) Wynne, K.; Reid, G. D.; Hochstrasser, R. M. *J. Chem. Phys.* **1996**, *105*, 2287.
(77) Asahi, T.; Ohkohchi, M.; Mataga, N. *J. Phys. Chem.* **1993**, *97*, 13152.
(78) Rathore, R.; Lindeman, S. V.; Kochi, J. K. *J. Am. Chem. Soc.* **1997**, *119*, 9393.
(79) Gould, I. R.; Farid, S. *Acc. Chem. Res.* **1996**, *29*, 522.